



OPEN ACCESS

EDITED BY
Ahmed Esmat Abdel Moneim,
Helwan University, Egypt

REVIEWED BY
Ziwei Huang,
Guangzhou University of Chinese
Medicine, China
Rami B. Kassab,
Helwan University, Egypt
Sidra Naz,
Beth Israel Deaconess Medical Center
and Harvard Medical School,
United States

*CORRESPONDENCE
Qi Zhou,
zhouqi133@999.com.cn
Ziren Su,
suziren@gzucm.edu.cn

[†]These authors have contributed equally
to this work

SPECIALTY SECTION
This article was submitted to
Experimental Pharmacology and Drug
Discovery,
a section of the journal
Frontiers in Pharmacology

RECEIVED 08 June 2022
ACCEPTED 24 October 2022
PUBLISHED 10 November 2022

CITATION
Xu L, Cheng J, Lu J, Lin G, Yu Q, Li Y,
Chen J, Xie J, Su Z and Zhou Q (2022),
Integrating network pharmacology and
experimental validation to clarify the
anti-hyperuricemia mechanism of
cortex phellodendri in mice.
Front. Pharmacol. 13:964593.
doi: 10.3389/fphar.2022.964593

COPYRIGHT
© 2022 Xu, Cheng, Lu, Lin, Yu, Li, Chen,
Xie, Su and Zhou. This is an open-access
article distributed under the terms of the
Creative Commons Attribution License
(CC BY). The use, distribution or
reproduction in other forums is
permitted, provided the original
author(s) and the copyright owner(s) are
credited and that the original
publication in this journal is cited, in
accordance with accepted academic
practice. No use, distribution or
reproduction is permitted which does
not comply with these terms.

Integrating network pharmacology and experimental validation to clarify the anti-hyperuricemia mechanism of cortex phellodendri in mice

Lieqiang Xu^{1†}, Juanjuan Cheng^{2†}, Jieyi Lu², Guoshu Lin²,
Qiuxia Yu³, Yucui Li², Jiannan Chen², Jianhui Xie³, Ziren Su^{2*}
and Qi Zhou^{2,4*}

¹College of Bioscience and Bioengineering, Jiangxi Agricultural University, Nanchang, China, ²School of Pharmaceutical Sciences, Guangzhou University of Chinese Medicine, Guangzhou, China, ³The Second Affiliated Hospital of Guangzhou University of Chinese Medicine, Guangzhou, China, ⁴China Resources Sanjiu Medical & Pharmaceutical Co., Ltd., Shenzhen, China

Hyperuricemia (HUA), a common metabolic disease, is treated as the second-largest metabolic disease after diabetes in China. Cortex Phellodendri (CP) is one of the most frequently used herbal medicines for treating gout or HUA. However, the mechanism underlying the anti-HUA effect of CP is still unrevealed. Hence, this study aimed to explore the pharmacological mechanism of CP against HUA using network pharmacology coupled with *in vivo* experimental validation. Active compounds and potential targets of CP, as well as the potential targets related to HUA, were retrieved from multiple open-source databases. The drug-disease overlapping targets were obtained by Venn diagram analysis and used to construct the herb-component-target (HCT), protein-protein-interaction (PPI), and component-target-pathway (CTP) networks. The functional enrichment analysis was also performed for further study. Furthermore, a HUA mouse model was induced by a combination of intraperitoneal injection of potassium oxonate (PO, 300 mg/kg) and intragastric administration of hypoxanthine (HX, 300 mg/kg) daily for 10 days. Different dosages of CP (200, 400, and 800 mg/kg) were orally given to mice 1 h after modeling. The results showed that 12 bioactive compounds and 122 drug-disease overlapping targets were obtained by matching 415 CP-related targets and 679 HUA-related targets, and berberine was one of the most important compounds with the highest degree value. The core targets of CP for treating HUA were TP53, MAPK8, MAPK3, IL-6, c-Jun, AKT1, xanthine oxidase (XOD), and ATP-binding cassette subfamily G member 2 (ABCG2). The Kyoto Encyclopedia of Genes and Genomes (KEGG) enrichment results showed that the anti-HUA effect of CP mainly involved the pathways of inflammation and apoptosis, such as PI3K/Akt, TNF, MAPK, TLR, AMPK, NF- κ B, and NLRP3 signaling pathways. *In vivo* animal experiment further confirmed the hypouricemic effect of CP in a HUA mouse model, as evidenced by significantly restored kidney histological deteriorations, and considerably decreased levels of serum uric acid (sUA), creatinine (Cre), blood urea nitrogen (BUN), and hepatic UA. Furthermore, the

hypouricemic action of CP *in vivo* might be attributed to its suppression of XOD activity in the liver, rather than ABCG2 in the kidney. Real-time qPCR (RT-qPCR) and Western blot analysis also confirmed the key roles of the hub genes in CP against HUA. In conclusion, CP exhibited therapeutic effect against HUA via multi-compounds, multi-targets, and multi-pathways. It possessed anti-HUA and nephroprotective effects via suppressing XOD activity, and reversed the progression of renal injury by exerting anti-inflammatory and anti-apoptotic effects.

KEYWORDS

Cortex Phellodendri, hyperuricemia, network pharmacology, berberine, xanthine oxidase

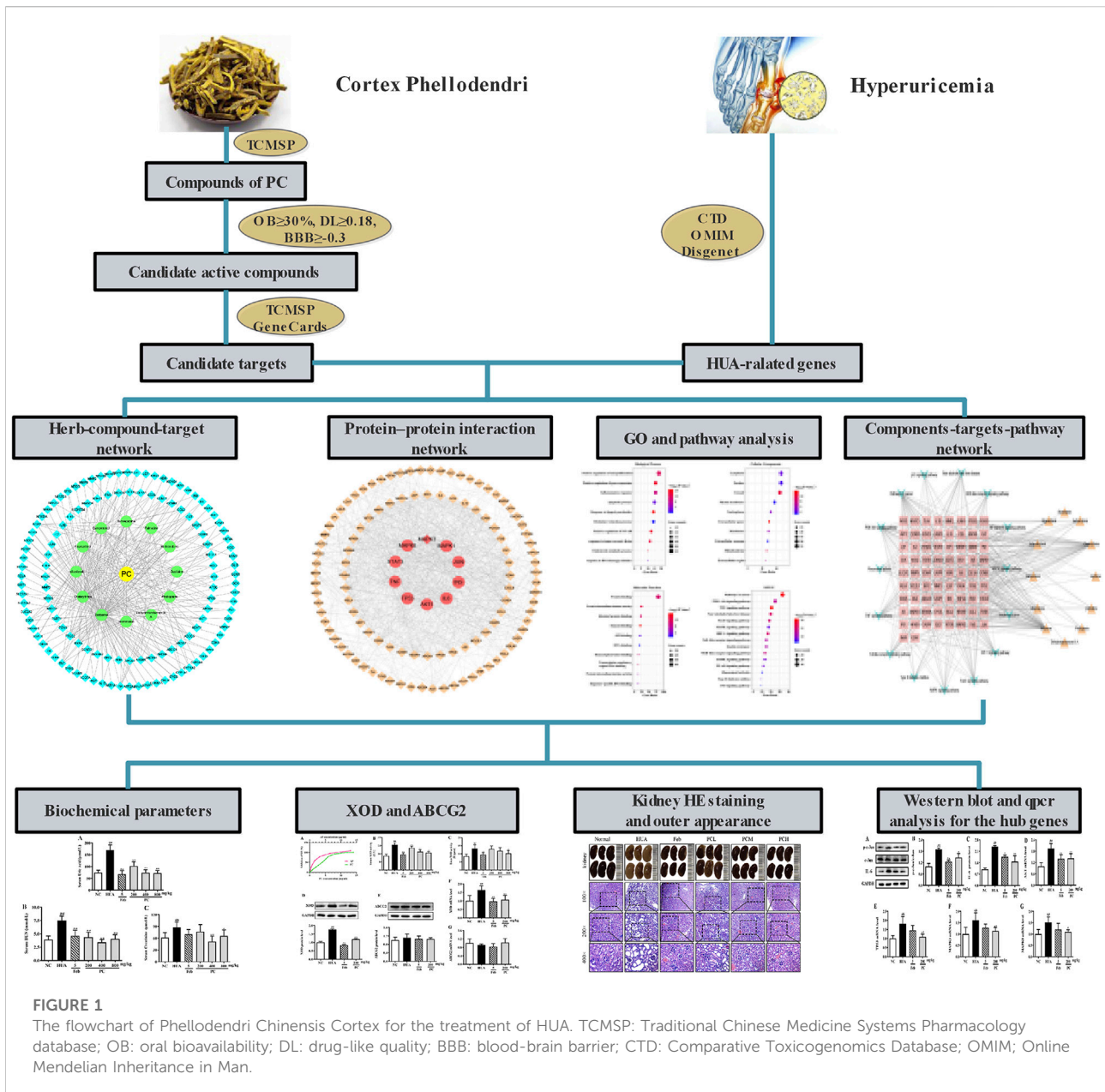
Introduction

Uric acid (UA) is the major final oxidation product of purine catabolism in humans and is formed by the catalytic action of xanthine oxidase (XOD). XOD is a key enzyme in the liver that catalyzes the transformation of hypoxanthine to xanthine and then to UA (Zhang et al., 2018). The presence of an increased UA level may be due to excessive production or decreased excretion, which is a sign of hyperuricemia (HUA). The cut-off value of 360 $\mu\text{mol/L}$ for women and 420 $\mu\text{mol/L}$ for men has been proposed to define HUA, considering the risk of monosodium urate crystal (MSU) formation increases when the sUA level exceeds the saturation threshold (Bardin and Richette, 2014). Excessive MSU deposits in the joints and soft tissues, triggering gout, tophi formation, kidney stones, and acute kidney failure (Richette and Bardin, 2010). Moreover, HUA is also closely related to the development of diabetes, kidney disease, hypertension, cardiovascular disease, and other diseases (Richette and Bardin, 2010). Urate-lowering therapy (ULT) has been widely adopted in the prevention and treatment of HUA and gout by reducing UA levels. However, most of the ULT agents in clinical practice have severe side effects or are ineffective for some patients (Pillinger and Mandell, 2020). Therefore, the development of effective and safe anti-HUA drugs remains an unmet clinical need.

Cortex Phellodendri (CP), also called “Huangbo” in Chinese, is a well-known Chinese medicine with two official monographs listed in the Chinese Pharmacopoeia: Cortex Phellodendron chinensis (CPC) and Cortex Phellodendron amurense (CPA) (Commission, C. P., 2020). CPC (known as “Chuanhuangbo” in Chinese) is derived from the dried bark of *Phellodendron chinense* Schneid. and is mainly distributed in the southwest part of China. CPA (known as “Guanhuangbo” in Chinese) is derived from the dried bark of *Phellodendron amurense* Rupr. and is mainly distributed in the northeastern part of China. Generally, these two species are used interchangeably for the treatment of dysentery, jaundice, urinary infection, and skin eczema, especially HUA (Chen et al., 2010). CP is a core and fundamental herb utilized either

alone or in combination with other herbs to treat HUA. Ermiao wan (EMW), a famous traditional Chinese medicinal (TCM) herbal prescription containing *Atractylodes Rhizome* and Cortex Phellodendri at a rate of 1:1 (w/w), was originally recorded in “Dan Xi Xin Fa” by Zhu Danxi in the Yuan Dynasty. EMW has been used medicinally for centuries for the treatment of gout and HUA, and modern pharmacological studies have also confirmed the anti-HUA effect of EMW (Kong et al., 2004; Wei et al., 2018). Due to its excellent hypouricemic ability, Sanmiao wan (Wang et al., 2010), Simiao wan (Ma et al., 2015), Jiawei Simiao wan (Hua et al., 2012), and Tongfeng decoction (Wu et al., 2019) were all invented based on EMW and exhibited potent anti-HUA and anti-gout effects. CP is the core herb among these herbal formulas, however, only a few studies have reported its urate-lowering effect (Yang et al., 2005; Pan et al., 2008). And the detailed mechanism underlying the hypouricemic and nephroprotective effects of CP remains obscure.

TCM emphasizes a holistic and systematic theory of the occurrence and development of disease. TCM possesses advantages of multi-components and being applied with multiple targets as well as multi-pathways synergies in the treatment and prevention of diseases (Wang et al., 2020). The emerging network pharmacology is a reliable and efficient approach for TCM pharmacological research. And it has been widely applied to predict the complex mechanisms of TCM from a comprehensive perspective, which is in line with the holistic view, systematic approach, and compatibility principle of TCM (Berger and Iyengar, 2009; Dong et al., 2021). In this work, a network pharmacology approach was adopted to analyze the active ingredients, specific targets, and underlying molecular mechanisms of CP against HUA. Furthermore, a HUA mouse model was also constructed to assess the therapeutic effect of CP and to verify the potential molecular mechanism predicted by network pharmacology. These results not only shed light on the molecular mechanisms of CP for treating HUA, but also provided scientific evidence to support the expansion of its use in clinical applications. The workflow is shown in Figure 1.



Materials and methods

Reagents and materials

Potassium oxonate (PO, purity >97%, Cat#: 156124) and hypoxanthine (HX, purity >99%, Cat#: H9377) were bought from Sigma-Aldrich Chemical Co. (St. Louis, MO, United States). Febuxostat (Feb, purity >98%, Cat#: S42697) was purchased from Shanghai Yuanye Bio-Technology Co., Ltd. (Shanghai, China). Allopurinol (AP, purity >98%, Cat#: 204337) was purchased from Hebei Bailing Weichao Fine Materials Co., Ltd. (Langfang, China). UA assay kits that used

the enzymatic-colorimetric method (Cat#: C012-2-1), Cre assay kits that used the sarcosine oxidase method (Cat#: C011-2-1), and BUN assay kits that used the urease method (Cat#: C013-2-1) were purchased from Nanjing Jiancheng Bioengineering Institute (Nanjing, China). The BCA protein determination kit (Cat#: P0012) was purchased from Beyotime Biotechnology (Shanghai, China). The following primary antibodies: rabbit anti-c-Jun pAb (Cat#: 24909-1-AP), rabbit anti-p-c-Jun pAb (Cat#: 28891-1-AP), rabbit anti-ABCG2 pAb (Cat#: 27286-1-AP), and anti-GAPDH pAb (Cat#: 10494-1-AP) were obtained from Proteintech Group, Inc. (Wuhan, China). Rabbit anti-XOD mAb (Cat#: ab109235), rabbit anti-IL-6 mAb (Cat#: ab233706),

TABLE 1 Sequences of the primers.

Description	Genebank	Sequence of primers (5'-3')	Product size (bp)	Tm (°C)
XOD	NM_011723	ATGACGAGGACAACGGTAGAT	185	55.3
		TCATACTTGGAGATCATCACGGT		55.0
ABCG2	NM_011920	CATCACATCACCTATCGAGTGA	172	53.7
		CTTTCCTTGCTGCTAAGACATC		53.5
AKT1	NM_001331107	ATGAACGACGTAGCCATTGTG	116	55.3
		TTGTAGCCAATAAAGGTGCCAT		54.1
MAPK3	NM_011952	CAGCTCAACCACATTCTAGGTA	158	53.9
		TCAAGAGCTTTGGAGTCAGATT		53.2
MAPK8	NM_001310452	CGCCTTATGTGGTGACTCGCTAC	102	60.5
		CTCCCATGATGCACCCAAGTAC		61.0
TP53	NM_001127233	ACCGCCGACCTATCCTTACCATC	89	61.2
		GGCACAAACACGAACCTCAAAGC		59.8
GAPDH	NM_001289726	GGTTGTCTCCTGCGACTTCA	183	57.5
		TGGTCCAGGGTTTCTTACTCC		56.5

and the second antibody anti-rabbit IgG (Cat#: ab6721) were purchased from Abcam (Cambridge, MA, United States). All other reagents were at least of analytical grade.

Preparation of ethanol extract

CPC was purchased from the First Affiliated Hospital of Guangzhou University of Chinese Medicine (GZUCM), Guangzhou, China. The herbal materials were extracted according to our previously published method (Xian et al., 2013). Briefly, the dried herbal material was crushed into powder by a pulverizer, passed through a 40-mesh screen, and 100 g of powder was refluxed with 800 ml of 80% aqueous ethanol for 1 h. The extraction procedure was then repeated twice more. The extract was pooled, filtered, and concentrated under reduced pressure in a rotary evaporator, followed by freeze-drying. The crude ethanol extract was resuspended in 0.5% sodium carboxymethyl cellulose (CMC-Na) for subsequent intragastric administration. The components of CPC extract have been detected and analyzed using high performance liquid chromatography, and the results have been shown in previous publication (Xian et al., 2013).

Screening potential bioactive compounds and targets

The main active compounds of CP were collected from the TCMSP database (<https://old.tcmsp-e.com/tcmsp.php>) (Ru et al., 2014), the TCM Database@Taiwan (<http://tcm.cmu.edu.tw>)

(Chen, 2011), and the TCMID database (<http://www.megabionet.org/tcmid/>) (Huang et al., 2018). According to the general filtering criteria suggested by TCMSP, the active compounds with OB \geq 30%, DL \geq 0.18 and BBB \geq -0.3 were screened out for further research. Then the potential targets of the active substances of CP were identified by the TCMSP, SwissTargetPrediction (<http://www.swisstargetprediction.ch/>) (Daina et al., 2019) and Gene Cards databases (<http://www.genecards.org/>) (Safran et al., 2002). All targets were restricted to human origins. All filtered targets were further normalized to official gene symbols using the UniProt database (<http://www.uniprot.org/>) (UniProt Consortium, 2019). Genes with missing annotations and duplicate genes were removed.

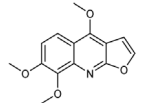
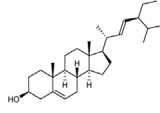
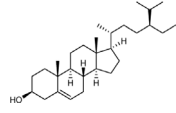
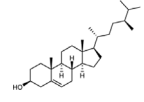
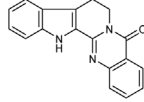
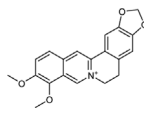
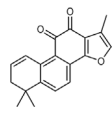
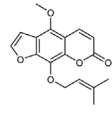
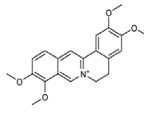
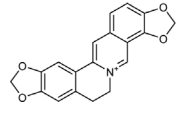
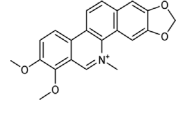
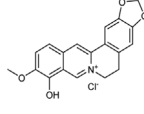
Screening potential disease targets of HUA

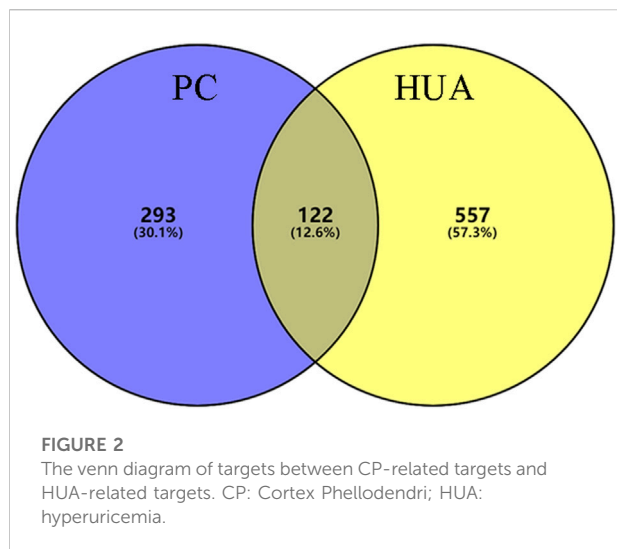
Here we applied the keyword of hyperuricemia to retrieve the related targets of disease in the following databases: CTD (<http://ctdbase.org/>) (Davis et al., 2021), OMIM (<https://omim.org/>) (Amberger et al., 2015), and DisGeNET (<https://www.disgenet.org/>) (Piñero et al., 2020). The overlapping targets between HUA and active compounds were obtained and visualized by the Venny (<https://bioinfogp.cnb.csic.es/tools/venny/>) online tools. The overlapping target set was considered the potential target of CP associated with HUA.

GO and KEGG pathway enrichment analysis

Gene Ontology (GO) terms and Kyoto Encyclopaedia of Genes and Genomes (KEGG) pathway enrichment analyses were assessed using the DAVID Bioinformatics Resources 6.8 (<https://david.ncifcrf.gov/>). The results were visualized as bubble charts using the RStudio software.

TABLE 2 Information of bioactive compounds of CP.

No.	Mol ID	Molecule name	OB (%)	DL	BBB	Caco-2	Structure
1	MOL002663	Skimmianin	40.14	0.20	1.10	1.26	
2	MOL000449	Stigmasterol	43.83	0.76	1.00	1.44	
3	MOL000358	β -sitosterol	36.91	0.75	0.99	1.32	
4	MOL005438	Campesterol	37.58	0.71	0.95	1.34	
5	MOL002662	Rutaecarpine	40.30	0.60	0.71	1.13	
6	MOL001454	Berberine	36.86	0.78	0.57	1.24	
7	MOL002651	Dehydrotanshinone II A	43.76	0.40	0.52	1.02	
8	MOL002644	Phellopterin	40.19	0.28	0.48	0.98	
9	MOL000785	Palmatine	64.6	0.65	0.37	1.33	
10	MOL001458	Coptisine	30.67	0.86	0.32	1.21	
11	MOL002666	Chelerythrine	34.18	0.78	0.28	1.24	
12	MOL002894	Berberrubine	35.74	0.73	0.17	1.07	



Network construction

To comprehensively elucidate the molecular mechanisms of CP in the treatment of HUA, the herb-component-target (HCT), protein-protein-interaction (PPI), and component-target-pathway (CTP) networks were constructed. Initially, to identify the core ingredients of CP treatment, the HCT network was established based on the active ingredients and overlapping genes. Furthermore, these overlapping genes were imported into the String database version 11.0 (<https://string-db.org/>) with Homo sapiens as the organism and a high confidence interaction score of >0.7 . The interaction results were exported as a “TSV” format and imported into Cytoscape software 3.7.1 for building a PPI network and network analysis. Finally, on the basis of the HCT network and KEGG pathway analyses, the effective components, targets, and top 15 pathway information were imported to Cytoscape software to construct the CTP network. The topological structure of networks was analyzed using the Network Analyzer and the CytoHubba plugin. The core ingredients and genes were ranked by degree value.

Animals

Six-to eight-week-old male ICR mice, weighing 18–22 g, were obtained from the Laboratory Animal Center of GZUCM. Before performing any experimental procedure, all mice were supplemented with a regular diet and allowed to drink *ad libitum* for 7 days to adapt to the controlled environment ($22 \pm 2^\circ\text{C}$, $60 \pm 10\%$ relative humidity, fixed 12-h artificial photoperiod). The animal experimental procedures were approved by the Animal Ethics Committee of GZUCM.

After acclimatization for 1 week, 72 male animals were assigned to 6 groups ($n = 12/\text{group}$): normal control (NC), HUA, febuxostat (5 mg/kg), and CP group (200, 400, and

800 mg/kg). To establish a hyperuricemic mouse model, all animals except normal mice were administrated with 300 mg/kg HX orally and 300 mg/kg PO intraperitoneally for 10 days. Mice in NC group mice were administered orally with an equal amount of normal saline (NS, 0.9%). One hour after modeling, animals in the treatment groups were orally given three doses (200, 400, and 800 mg/kg) of CP, while mice in the NC and HUA groups were given equal amounts of NS instead. Febuxostat was given as a positive control. All animals were anesthetized with pentobarbital sodium (60 mg/kg) 4 h after CP treatment on day 10. All efforts were made to minimize suffering. The blood samples were collected by retro-orbital bleeding for serum preparation. Tissues were rapidly dissected out, rinsed, blotted dry, weighed, frozen in liquid nitrogen, and then stored at -80°C until processed.

Biochemical assays

The whole blood was centrifuged at 3500 rpm for 10 min at 4°C immediately after blood collection. The supernatant containing the serum was collected and then analyzed immediately for levels of UA, BUN, Cre, and XOD activity using appropriate commercial kits according to the manufacturer’s protocols.

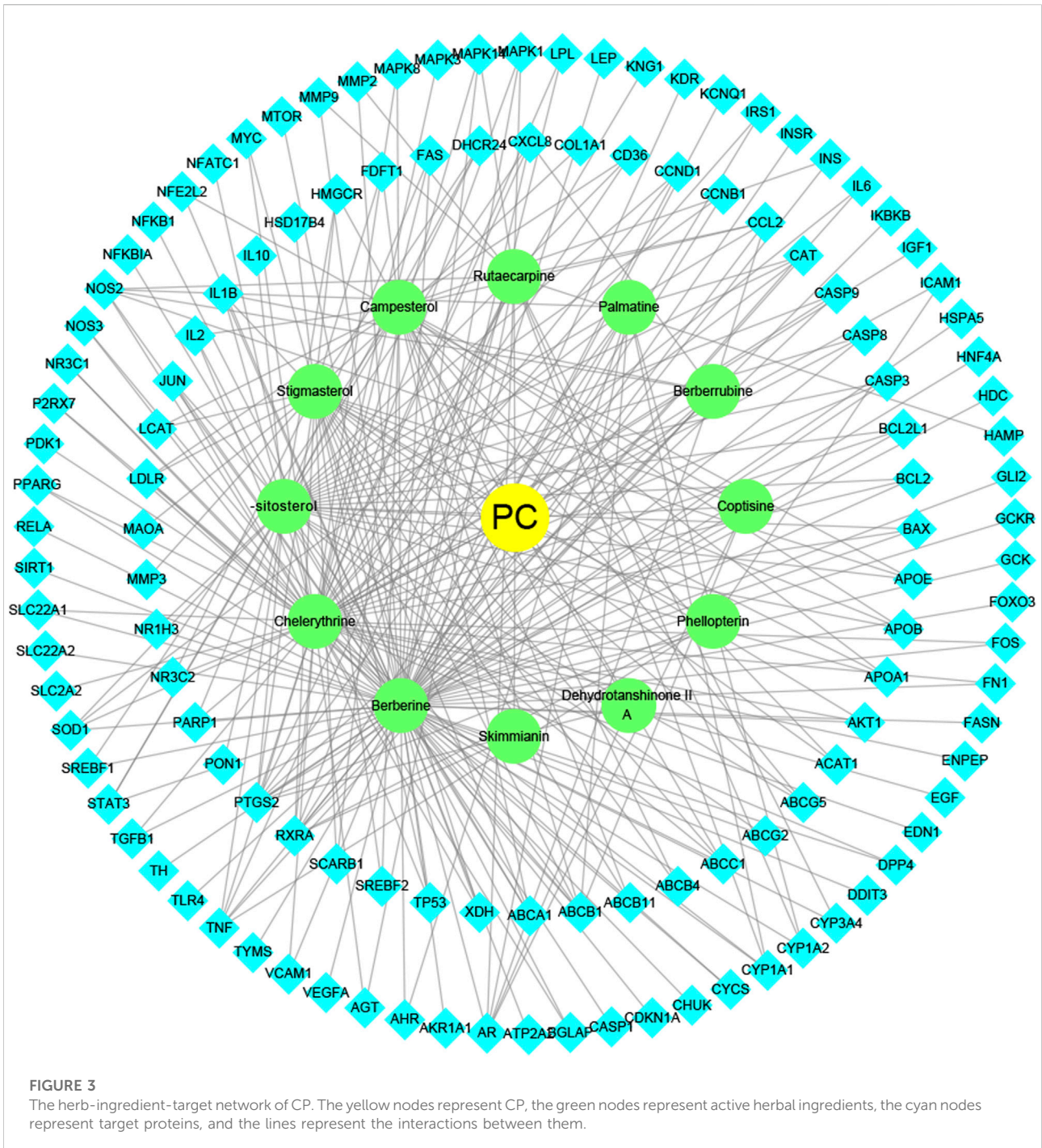
The liver tissues were homogenized in NS for 3 min at a ratio of 10% w/v using a homogenizer. The homogenate was centrifuged at 3,000 rpm at 4°C for 15 min. The total protein concentration was measured with a BCA assay kit. The supernatant fraction was used to measure the UA level and XOD activity in the liver using appropriate commercial kits according to the manufacturer’s protocols.

Histological assays

The kidney tissues were fixed in 4% paraformaldehyde for 24 h at room temperature, and then routinely processed for paraffin embedding, sectioned at $5 \mu\text{m}$, and stained with hematoxylin-eosin (HE). Then the stained kidney slices were imaged under Olympus BX53 optical microscopy (Tokyo, Japan) at $100\times$, $200\times$, and $400\times$ magnification. Additionally, histopathological scores were assessed double-blindly according to the methods established by a previous study (Xu Y. et al., 2021). Generally, the method was based on glomerulopathy (0–4, from normal glomerular structure to most glomerular atrophy); tubulopathy (0–4, from normal structure of tubules to most tubule dilation); and renal interstitial inflammatory infiltration (0–4, from non-inflammatory cells to a large number of inflammatory cells).

XOD inhibition assay

An *in vitro* XOD inhibitory assay was conducted according to our published method with slight modifications (Xu L. Q. et al., 2021). Firstly, $20 \mu\text{L}$ XOD stock solution was diluted with $980 \mu\text{L}$



PBS (pH 7.4) to prepare a working stock enzyme solution. Xanthine powder was dissolved in PBS at a concentration of 7.6×10^{-2} mg/ml 50 μ L of CP solution (at concentrations of 0.5, 1, 2, 4, 6, 8, 10, 12, and 14 mg/ml), 77 μ L of PBS (pH 7.4) and 7 μ L of XOD enzyme solution were mixed and incubated at room temperature for 30 min. Then xanthine solution (66 μ L) was added to the mixture to initiate the reaction. The reaction

mixture was incubated in an oven at 37°C for 30 min, and the UV absorbance was measured at 290 nm. Allopurinol was used as a positive control. The XOD inhibitory activity was determined as follows:

$$XOD \text{ inhibitory activity } (\%) = \left[1 - \frac{(S - S_0)}{(B - B_0)} \right] \times 100$$

TABLE 3 Active ingredients and topological properties.

Compound	Degree	Betweenness	Closeness
Berberine	89	10,799.54	105.83
Chelerythrine	58	4732.711	85.17
β -Sitosterol	34	1927.92	69.17
Stigmasterol	29	2534.62	65.83
Campesterol	24	1154.68	62.50
Rutaecarpine	16	508.88	57.17
Palmitine	11	108.72	53.83
Berberubine	9	53.73	52.50
Coptisine	6	35.84	50.50
Phellopterin	5	31.78	49.83
Dehydrotanshinone II A	3	5.03	48.50
Skimmianin	2	0.56	47.83

Where S and S_0 are the absorbances of the reaction system with or without XOD, respectively. B is the absorbance of the reaction system without samples, B_0 is the absorbance of the reaction system without samples and XOD.

Western blotting

Mouse kidney total protein was prepared after homogenization of 100 mg tissues in RIPA buffer with a protease inhibitor cocktail, PMSF, and sodium orthovanadate. Thereafter, supernatants were collected after centrifugation at 12,000 rpm for 10 min at 4°C. The protein concentration was determined using a BCA kit. Equivalent amounts of protein (50 μ g/lane) from each group were resolved by 10% SDS-PAGE and then transferred to PVDF membranes by electroblotting. Subsequently, the membranes were blocked in 0.1% TBST containing 5% dried skim milk at room temperature for 1 h, and incubated with the following primary antibodies at 4°C overnight: anti-XOD (1:10,000), anti-ABCG2 (1:1,000), anti-IL-6 (1:1,000), anti-c-Jun (1:1,000), anti-p-c-Jun (1:1,000). Following overnight incubation, primary antibodies were removed and the membranes were rinsed three times with TBST for 10 min each. Next, the membranes were incubated with secondary HRP-conjugated goat anti-rabbit IgG (Immunoglobulin G, 1:4,000) antibody at room temperature for 1 h. Protein bands were visualized by the ECL method and analyzed by ImageJ software (NIH, Bethesda, MA, United States).

RT-qPCR

Total RNA from an appropriate amount of preserved kidney and liver was extracted using Trizol reagent (Life Technologies, Inc.). Briefly, tissues (0.10 g) were first homogenized in 1 ml Trizol solution, and the homogenate was mixed with 200 μ L chloroform and centrifuged at 12,000 rpm for 15 min at 4°C. The aqueous phase was

reserved, precipitated with isopropanol (1:2, v/v), and centrifuged at 10,000 rpm for 10 min. Finally, the RNA was washed with 70% ethanol and resuspended in 20 μ L of DEPC water. The quality and concentration of total RNA were measured using a NanoDrop-2000 spectrophotometer. Subsequently, total RNA (1 μ g) was subjected to cDNA synthesis using a HiScript II Q RT SuperMix for qPCR (+gDNA wiper) reagent kit (R223-01, Vazyme, Nanjing, China). Real-time PCR was performed with the SYBR Green Master Mix kit (Q711-02, Vazyme, Nanjing, China) according to the manufacturer's instructions in the CFX 96 Real-Time PCR Detection System (Bio-Rad, CA, United States). The PCR conditions were set as follows: 1 cycle of 95°C for 30 s; 40 cycles of 95°C for 10 s, 60°C for 30 min; 1 cycle of 95°C for 15 s followed by a melting curve step from 65°C to 95°C, 5 s per 0.5°C. The amplification data were evaluated based on the $2^{-\Delta\Delta Ct}$ method, and the results were normalized against β -actin. All primers used for RT-qPCR were synthesized by Sangon Biotech Company (Shanghai, China) (Table 1).

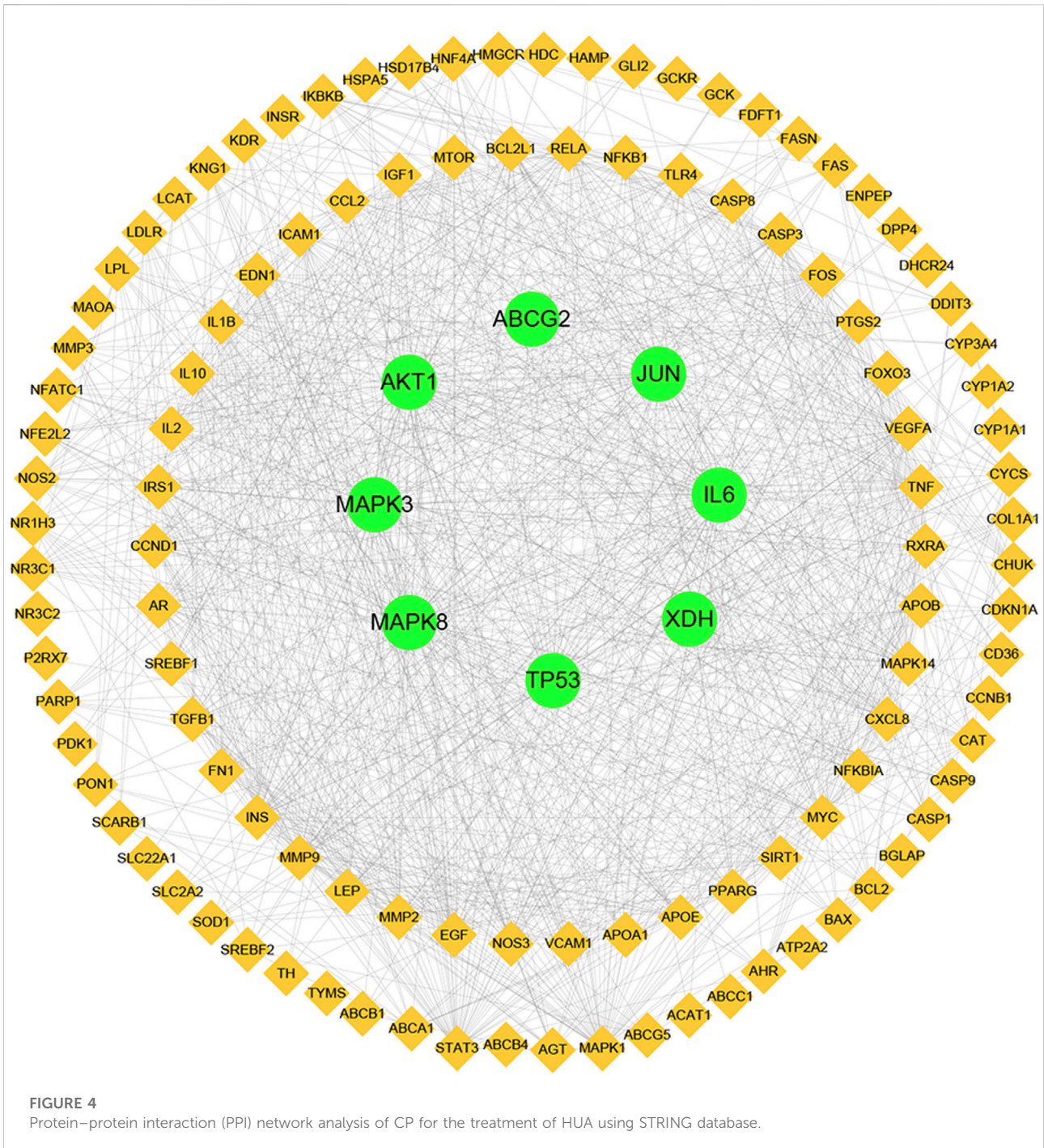
Statistical analysis

Data were given as mean \pm standard deviation (SD). All datasets were subjected to a normal distribution test first. If they followed normal distribution, one way analysis of variance (ANOVA) followed by Bonferroni post hoc test was used for comparisons, otherwise comparisons were performed using Kruskal–Wallis test. Statistical analyses and graphing were performed using SPSS (Version 19.0, IBM, United States) and GraphPad Prism (Version 6.0, GraphPad Software Inc., CA, United States), respectively. Statistical significance was set at $p < 0.05$.

Results

Identification of bioactive compounds and targets

In this study, 140 compounds were obtained from multiple databases. After screening by ADME parameters ($OB \geq 30\%$, $DL \geq 0.18$, and $BBB \geq -0.3$), 27 components were obtained, accounting for 19.29%. Furthermore, 27 components were input into the open-source databases to search for the corresponding targets, among which only 12 compounds were found to be the corresponding targets. These 12 compounds were deemed to be core bioactive components for further analysis, and the detailed information is shown in Table 2. Next, 415 targets interacting with the above 12 core compounds in CP were screened from the TCMSP and GeneCard databases (Supplementary Excel Sheet S1). Furthermore, by screening



CTD, OMIM, and DisGeNET databases, 679 HUA-related genes were fished out (Supplementary Excel Sheet S2). Integration of the targets regulated by core compounds and the targets related to HUA revealed that 122 genes overlapped (Figure 2). Therefore, it was reasonable for us to consider that these common genes were the potential therapeutic targets of CP in HUA.

HCT network construction and analysis

To intuitively visualize the interaction correlation between the core bioactive components and the common genes, the HCT network was established by Cytoscape 3.7.1. As shown in Figure 3, the network comprised 489 nodes and 974 interactions. After the network was analyzed by its plugin,

TABLE 4 Hub genes and topological properties.

Gene	Degree	Betweenness	Closeness
<i>AKT1</i>	64	0.10572	0.64641
<i>IL6</i>	56	0.05602	0.62234
<i>TP53</i>	55	0.09232	0.61579
<i>MAPK8</i>	55	0.04456	0.60622
<i>Jun</i>	53	0.03729	0.59391
<i>MAPK3</i>	43	0.02741	0.570732
<i>ABCG2</i>	6	0.03560	0.43173
<i>XDH</i>	2	0.00063	0.33429

the Network Analyzer, components were ranked by degree value in descending order. As shown in Table 3, berberine was found to have the highest degree value (degree = 89), suggesting that berberine might be the most critical ingredient for CP against HUA.

PPI network construction and analysis

Next, a PPI network was built using the STRING database and Cytoscape software. As shown in Figure 4, the network comprised 118 nodes and 1079 links. The plug-in “CytoHubba” was used to analyze the topological properties of the PPI network, including degree, closeness centrality, and betweenness centrality (BC). The top 10 genes in each topological algorithm were compared, and the overlapped genes in these three topological parameters were selected as the key genes for further analysis (Table 4).

Enrichment analysis

To explore the potential pharmacological actions of CP, the online database DAVID was utilized to carry out GO and KEGG annotation. The top 10 significantly enriched GO terms and top 15 KEGG pathways were plotted as bubble charts using the R package ggplot2. As shown in Figure 5, the biological process (BP) was significantly enriched in positive regulation of cell proliferation and gene expression, inflammatory response, and apoptotic process, etc. Cellular component (CC) was significantly enriched in cytoplasm, nucleus, cytosol, plasma membrane, and nucleoplasm, etc. Molecular function (MF) was significantly enriched in protein binding and homodimerization activity, identical protein binding, enzyme binding, and ATP binding, etc. Moreover, KEGG enrichment analysis indicated that 122 overlapping genes were significantly enriched in inflammation and apoptosis signaling pathways, including PI3K/AKT, TNF, FoxO, MAPK, HIF-1, TLR, NLRP3, AMPK, and NF- κ B, etc.

CTP network construction and analysis

As shown in Figure 6, the CTP network comprised 101 nodes and 468 links. According to the network analysis, one pathway and compound could act on multiple targets, and one target could act on multiple pathways and compounds. This network diagram fully reflected the characteristics of the synergistic relationship between multiple components, targets, and pathways of CP treatment of HUA.

Effects of CP on body weight and organ index

No deaths were observed in any mice during the course of the study. No significant differences were seen in body weight, liver weight, or liver index among the experimental groups (Table 5). While kidney and spleen weights and indexes were significantly higher in the HUA group than those in the NC group ($p < 0.05/0.01$). CP treatment dramatically decreased the kidney weight and kidney indexes ($p < 0.01$). However, CP did not cause any significant reduction in the spleen weight or spleen index.

Effects of CP on liver UA, serum UA, cre, and BUN levels

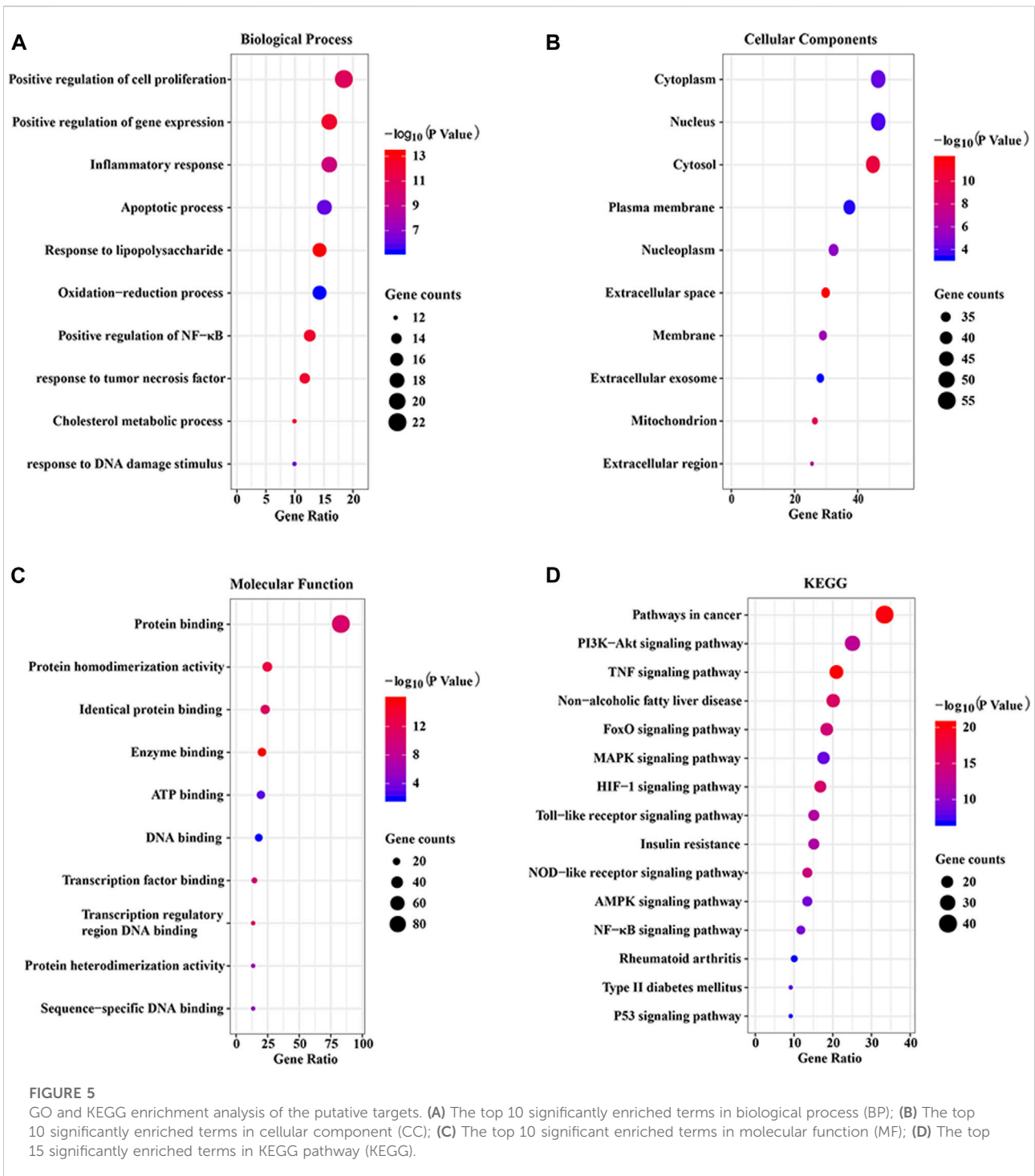
As indicated in Figure 7A, compared to the NC group, a nearly 126.7% increase in sUA level was noted in HUA mice induced by HX combined with PO ($p < 0.01$), indicating the HUA model was successfully constructed. CP and Feb treatment remarkably decreased the sUA level in HUA mice ($p < 0.01$). Feb decreased the sUA level by 59.8% and three-dose CP groups decreased the sUA level by approximately 39.5%, 56.3%, and 57.3%, respectively.

In addition, as shown in Figure 7B, PO/HX induced a remarkable elevation in liver UA levels in mice compared to the NC group mice ($p < 0.01$). Feb, a positive control drug, significantly decreased UA level in the liver compared with the HUA group ($p < 0.01$). Compared with the HUA group, the UA level in the liver was significantly reduced by CP at doses of 400 and 800 mg/kg ($p < 0.01$), respectively.

As shown in Figures 7C,D, compared with the NC group, the serum Cre and BUN levels in the HUA group were observably increased by 42.6% and 90.9%, respectively ($p < 0.01$). Nonetheless, both serum Cre and BUN levels were remarkably reduced after CP treatment ($p < 0.05/0.01$), indicating that CP could alleviate kidney injury in HUA mice.

XOD inhibition assay *in vitro* and *in vivo*

As shown in Figure 8A, the activity of XOD was inhibited by CP extract *in vitro* in a dose-dependent manner, and the IC_{50} of CP extract was 3.34 mg/ml. While the IC_{50} of the positive control, allopurinol, was 1.08×10^{-3} mg/ml.



In vivo, compared to the NC group, the serum and liver XOD levels in the HUA group were significantly increased by 77.3% ($p < 0.01$) and 55.3% ($p < 0.01$), respectively (Figures 8B,C). However, CP administration effectively decreased serum XOD activity by approximately 12.2%, 27.0% and 31.5% (all $p < 0.05$), respectively. And the mice treated with 800 mg/kg of CP

exhibited a significant reduction in liver XOD activity by 21.7% ($p < 0.05$).

The XOD mRNA and protein levels were assessed via RT-qPCR and Western blot analyses. Compared to the NC mice, the relative expression of XOD protein (Figure 8D) and mRNA (Figure 8F) was significantly increased in the HUA mice (all $p < 0.01$), while CP

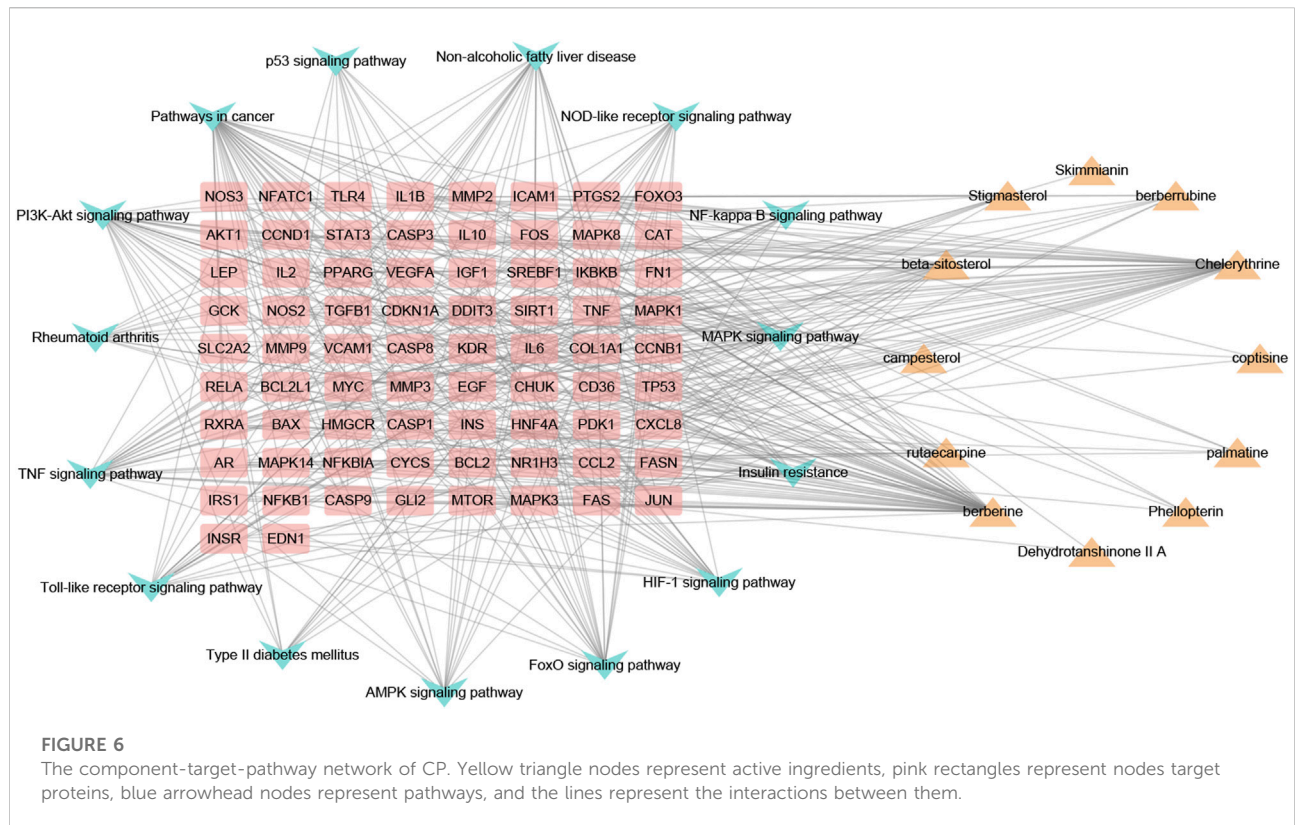


TABLE 5 Effect of CP on body weight, organ weight and organ index.

Group	Body weight (g)	Organ weight (g)			Organ index (%)		
		Liver	Kidney	Spleen	Liver	Kidney	Spleen
NC	27.80 ± 2.92	1.37 ± 0.11	0.30 ± 0.07	0.067 ± 0.016	4.96 ± 0.52	1.06 ± 0.14	0.24 ± 0.05
HUA	27.14 ± 3.20	1.41 ± 0.17	0.53 ± 0.07##	0.091 ± 0.017#	5.22 ± 0.58	1.97 ± 0.38##	0.34 ± 0.06##
Feb (5)	28.78 ± 2.35	1.46 ± 0.11	0.32 ± 0.04**	0.081 ± 0.014	5.08 ± 0.34	1.10 ± 0.14**	0.28 ± 0.05
CP (200)	28.23 ± 2.36	1.48 ± 0.12	0.32 ± 0.06**	0.095 ± 0.014	5.23 ± 0.49	1.12 ± 0.24**	0.34 ± 0.03
CP (400)	28.85 ± 2.40	1.44 ± 0.13	0.29 ± 0.03**	0.095 ± 0.011	5.12 ± 0.61	1.01 ± 0.16**	0.33 ± 0.04
CP (800)	28.96 ± 2.20	1.45 ± 0.18	0.28 ± 0.05**	0.100 ± 0.020	4.96 ± 0.56	0.97 ± 0.20**	0.35 ± 0.07

The results are expressed as mean ± SD (n = 10). #p < 0.05, ##p < 0.01 compared with NC, group; *p < 0.05, **p < 0.01, compared with HUA, group.

administration distinctly reversed these effects (p < 0.01). As expected, Feb also significantly reduced the mRNA and protein levels of XOD in HUA mice.

Effects of CP on renal ABCG2 expression level

The mRNA and protein expression of ABCG2 in the kidney was assessed. As revealed in Figure 8E & G, no differences were observed among the experimental groups.

Effects of CP on kidney histopathological changes

In Figure 9, the kidneys from the NC group showed a reddish, shiny, and elastic appearance. HE staining results indicated that the kidney in the NC group presented a normal architecture with an intact glomerulus and renal tubules. However, the gross appearance of the kidney in the HUA group was pale and irregularly shaped. HE-stained kidney sections of the HUA model group also revealed a marked renal injury, as manifested by severe tubular

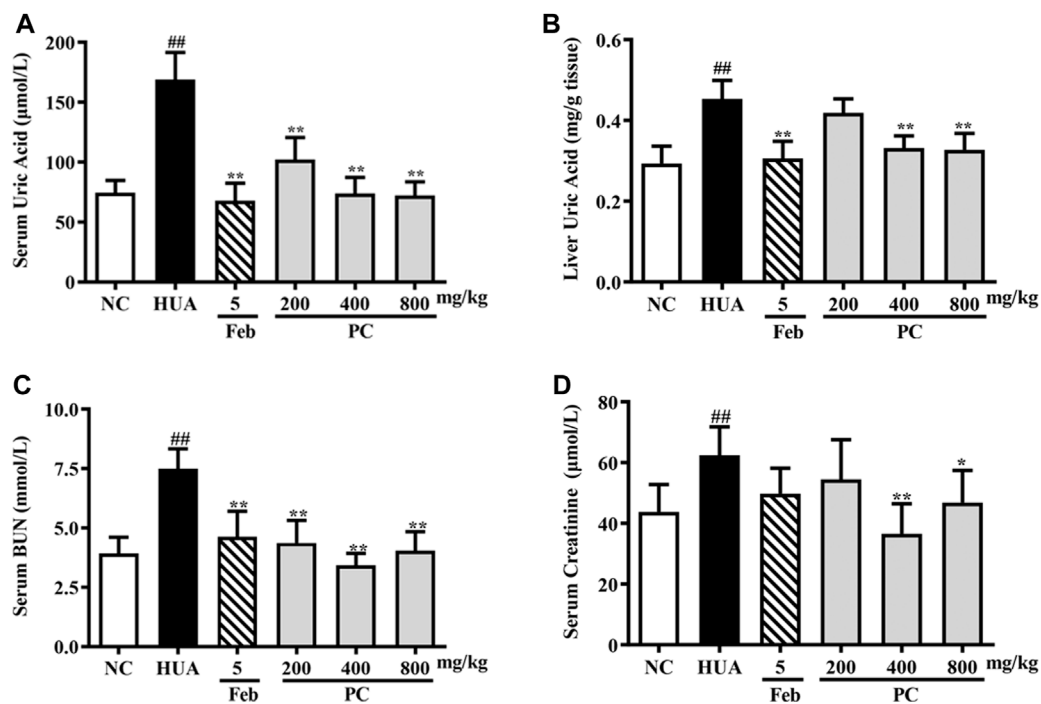


FIGURE 7

Effects of CP on liver UA, serum UA, Cre, and BUN levels in PO/HX-induced HUA mice. (A) The serum level of UA. (B) The liver level of UA. (C) The serum level of BUN. (D) The serum level of Cre. The results are expressed as mean \pm SD ($n = 10$). ^{##} $p < 0.01$ compared with NC group; ^{*} $p < 0.05$, ^{**} $p < 0.01$ compared with HUA group.

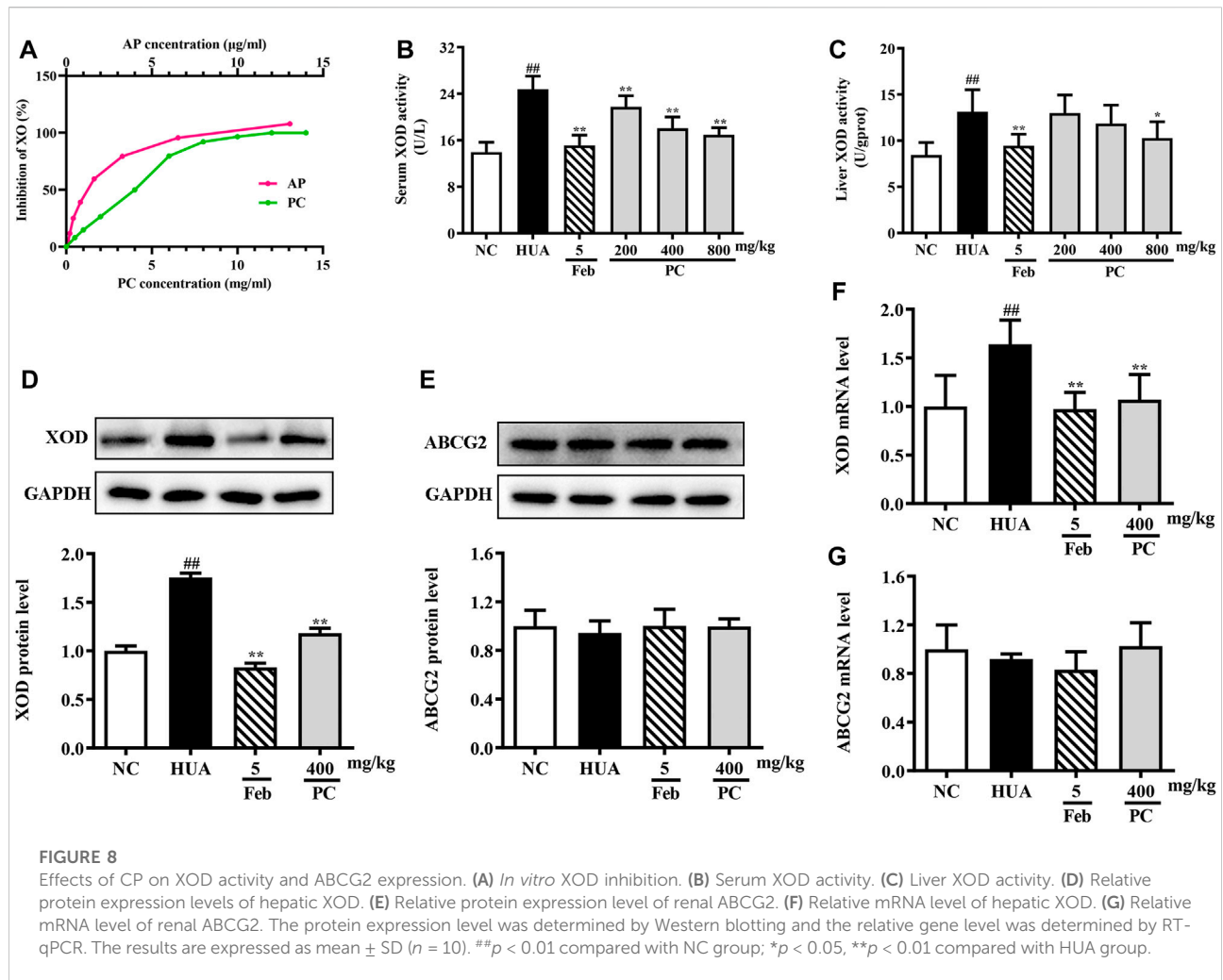
dilation, mild inflammatory cell infiltration, renal tubules with protein casts, swelling, and proximal tubule necrosis. Feb and CP administration effectively mitigated the renal injury, and the renal protective effect of CP was dose-dependent. The histopathological scores of kidneys in the HUA group were significantly higher than those in the NC group ($p < 0.01$). The histopathological scores of the kidney from mice in Feb and PC groups were significantly lower than those from mice in the model group ($p < 0.01$).

Effects of CP on the expression of hub genes

To further validate the effects of CP on the hub genes predicted by network analysis, the mRNA and protein expression levels were detected. As shown in Figure 10, the protein expression levels of p-c-Jun and IL-6, as well as the mRNA levels of *MAPK3*, *MAPK8*, *AKT*, and *TP53* were markedly up-regulated in the kidney tissues of HUA mice than in those of the NC mice ($p < 0.01$). Notably, CP treatment succeeded in restoring HUA-induced over-expression of the hub genes.

Discussion

HUA is a metabolic abnormality caused by urate overproduction, urate underexcretion, extra-renal urate excretion caused by *ABCG2* dysfunction, or both (Ichida et al., 2012; Dalbeth et al., 2016). To date, genome-wide association studies (GWAS) have found various genetic loci that influence sUA levels, such as *GLUT9*, *URAT1*, *NPT1*, and *ABCG2* (Nakatouchi et al., 2019). These genes are validated targets for several existing drugs that have been widely used in clinical practice for treating HUA and gout. Allopurinol and febuxostat are xanthine oxidase inhibitors (XOIs) that block the formation of UA and are recommended as the first-line pharmacologic urate-lowering agents. However, allopurinol can induce severe hypersensitivity syndrome (AHS) (Perez-Ruiz and Dalbeth, 2019). Febuxostat has been reported to be more effective at a fixed or limited dose (maximum 200–300 mg/day) in clinical trial, however accompanied by major adverse effects such as abnormal liver function and gout flares (Becker et al., 2005; Becker et al., 2009). Benzbromarone and lesinurad are considered the second-line ULTs for gout that lower sUA levels by inhibiting *URAT1*. However, lesinurad was not available in the United States due to a high incidence of renal side effects (Jansen et al., 2018), and benzbromarone is not licensed in

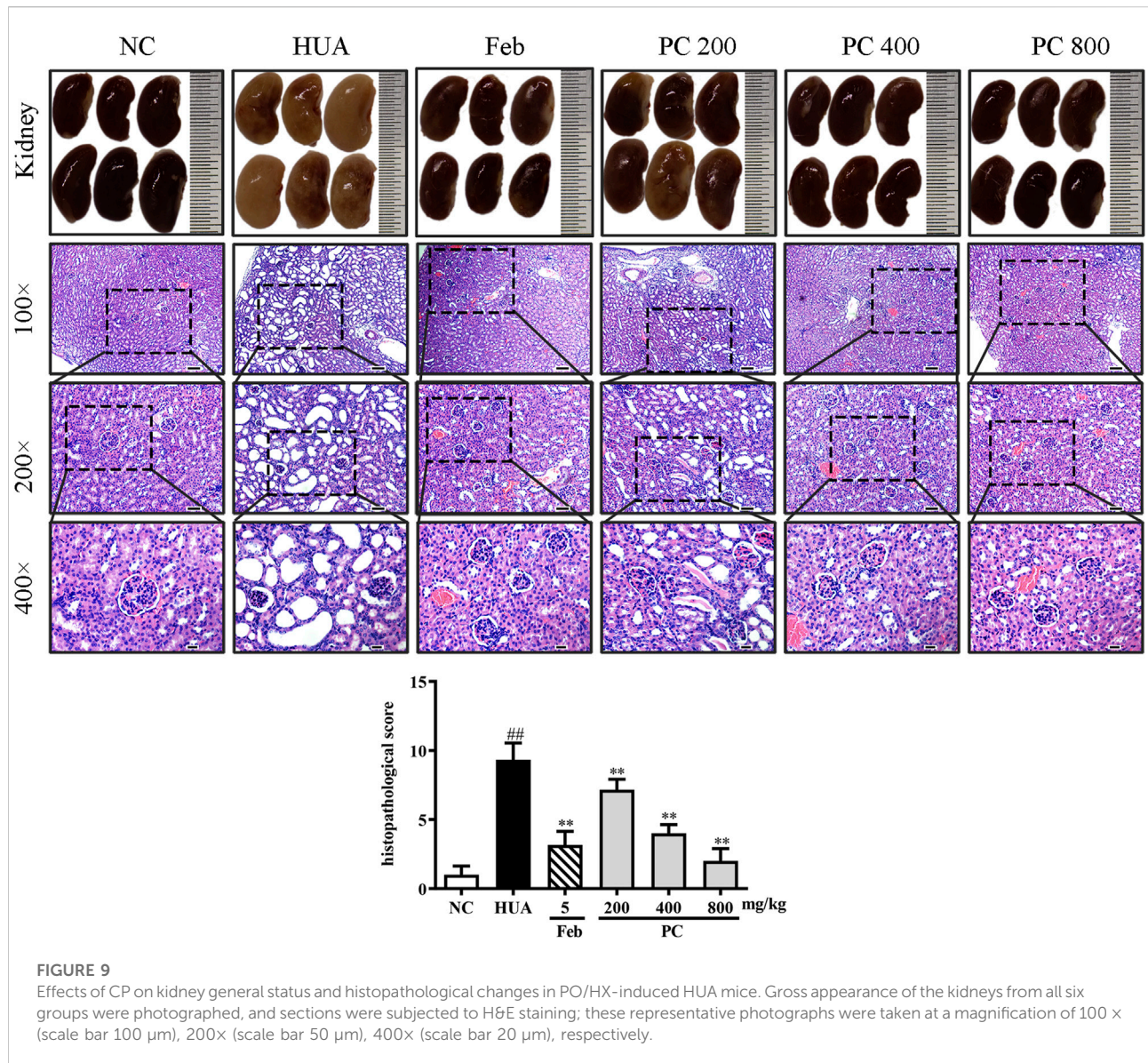


the United States due to concerns about its hepatotoxicity (Lee et al., 2008). Therefore, the development of anti-HUA drugs with high efficiency and mild or no side effects is badly needed. CP has been used as a core herb in China for the treatment of HUA for thousands of years. In the present study, network pharmacology methods and experimental validations were performed to further explore the potential mechanisms and therapeutic effects of CP on HUA for the first time. These findings laid the foundation for future clinical research in this area.

The serum UA level has been widely accepted as a reliable indicator of HUA, and the liver is the most critical organ for UA production. Hence, in this study, the serum and liver UA levels were determined. Our results revealed that administration with CP obviously attenuated the rise of UA levels in serum and liver. Besides, many studies have suggested that a high level of serum UA is closely related to renal dysfunction (Akioka et al., 2017). Serum BUN and Cre are the two most widely used indexes to assess renal function. Besides, several parameters, including kidney weight and index, and renal histopathology and morphology, were evaluated for the protective effect of CP

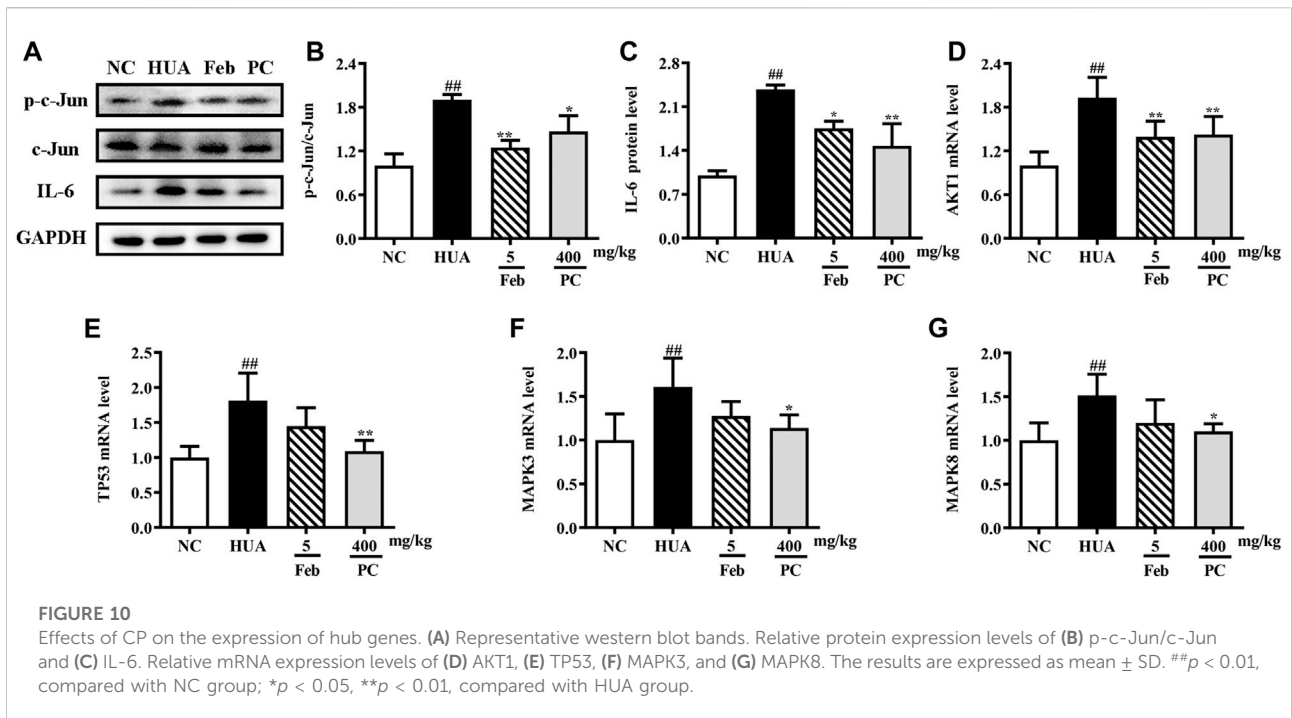
against HUA-induced renal toxicity. Results suggested that CP exerted promising nephroprotective effects in HUA mice, as evidenced by reduced kidney weight and index, decreased serum BUN and Cre levels, alleviated histopathological alterations, as well as normalized kidney morphology. Conclusively, CP exhibited remarkable ameliorative effects against PO/HX-induced HUA and renal injury.

In this study, 12 bioactive compounds of CP were screened out from the TCMSP database, 415 CP-related targets were selected from the TCMSP and Gene Cards databases, and 679 HUA-related genes were obtained from the OMIM, CTD, and DisGeNET databases. Then a total of 122 herb and disease co-target genes were obtained and adopted to establish an “HCT” network. In the network, the key bioactive ingredients such as berberine (degree 89), chelerythrine (degree 58), β-sitosterol (degree 34), stigmasterol (degree 29), campesterol (degree 24), rutaecarpine (degree 16), palmatine (11), and berberrubine (degree 9) had a high degree value. Berberine (BBR) is a naturally occurring isoquinoline alkaloid and the main effective compound of Phellodendri Cortex. Berberrubine



(BRB) is deemed as one of the main metabolites of BBR. Our previous study has indicated that BBR and BRB effectively lowered the sUA levels in PO/HX-induced HUA mice (Lin et al., 2021; Shi et al., 2021). Chelerythrine is a natural benzo [c]phenanthridine alkaloid derived from *Chelidonium majus*, *Macleaya cordata*, and *Sanguinaria canadensis* (Wu et al., 2018). It possesses anti-tumor (Zhang et al., 2011), anti-diabetes (Zheng et al., 2015), and anti-inflammatory properties (Niu et al., 2011), and protective effects against ethanol-induced gastric ulcer (Li et al., 2014) and lipopolysaccharide-induced endotoxic shock (Niu et al., 2014). Besides, chelerythrine is also beneficial for obstructive nephropathy (Juan et al., 2012; Shi et al., 2019). In most of the cases, β-sitosterol, campesterol, and stigmasterol are among the most common phyosterols,

which possess diverse pharmacological properties, including anti-cancer, anti-inflammatory, anti-oxidant, and blood lipid-lowering activities (Trautwein and Demonty, 2007). It has been reported that β-sitosterol is able to alleviate monosodium urate (MSU) crystal-induced paw oedema in mice (de Souza et al., 2012). Previous studies have demonstrated that stigmasterol can reduce sUA levels in HUA mice via inhibiting XOD activity and remarkably decrease the paw edema induced by MSU crystals (Ferraz-Filha et al., 2016). To our knowledge, the hypouricemic effects of rutaecarpine and palmatine have yet to be investigated. However, these compounds have been reported to show anti-inflammatory effects (Luo et al., 2020; Ma et al., 2021). Collectively, these findings suggest that CP displayed anti-HUA action via multiple ingredients that acted on multiple targets.



To further elucidate the molecular mechanisms, a PPI network containing 118 nodes and 1079 links was established using the common potential targets of CP and HUA. Then topological property analysis was performed, and the top 6 genes obtained by calculating the degree, betweenness, and closeness centrality algorithms were selected as hub genes: *TP53*, *MAPK8*, *MAPK3*, *IL-6*, *c-Jun*, and *AKT1*. However, due to the strict screening criteria, *XOD* and *ABCG2*, two common intersection targets of CP and HUA, were excluded. In view of their important roles in UA metabolism, the expression of *XOD* and *ABCG2* were also evaluated in this study. *XOD* is a key enzyme that catalyzes hypoxanthine into xanthine and then metabolizes xanthine to UA. *ABCG2* is a high-capacity transporter that facilitates UA excretion in the intestine and kidney (Woodward et al., 2009). In this study, CP exerted inhibitory activity on *XOD* *in vitro* by direct assay and *in vivo* by using a HUA mouse model. However, no significant difference was observed in kidney protein and mRNA levels of *ABCG2* among all groups, whereas the levels of *ABCG2* in intestinal samples were not examined and need to be explored further. Consistent with the foregoing result, *XOD* is a key target for CP to lower UA (Kong et al., 2004). *IL-6* acts mostly as a proinflammatory cytokine involved in the pathogenesis of gout, and may be a reliable prognostic marker for patients with gout (Cavalcanti et al., 2016). *TP53* (also known as p53) is a multi-functional tumor suppressor gene and functions as a transcriptional regulator that governs multiple cellular processes, such as cell cycle, DNA repair, apoptosis, and senescence. Previous studies have demonstrated that

p53 may be a key modulator of *IL-6* in the synovium and plays a prominent role in the inhibition of inflammation (Zhang et al., 2016). The most common proto-oncogene, *c-Jun*, is activated by various extracellular signals and serves important roles in cell proliferation, differentiation, apoptosis, and invasion. And the activation of *c-Jun* is also closely related to the regulation of inflammation and/or fibrosis in human renal disease (De Borst et al., 2007). *Akt1* is a crucial downstream effector of *PI3K/Akt* signaling and plays a role in the transcriptional modulation of a subset of genes associated with cell growth, proliferation, and apoptosis (Hixon and Boekelheide, 2003). Previous studies have reported that inhibition of activity of the *Akt1* protein could decrease the deposition of fibronectin and improve diabetic nephropathy (Hong et al., 2013). *MAPK3* (also known as *ERK1*) and *MAPK8* (also known as *ERK1*) are both mitogen-activated protein kinases that can mediate the progress of cell growth, differentiation, inflammatory response, proliferation, apoptosis, and other pathological processes. This study found that CP significantly inhibited the mRNA and protein expression of hepatic *XOD* in the HUA mice, as well as the expression of renal *TP53*, *MAPK8*, *MAPK3*, *IL-6*, *c-Jun*, and *Akt1* at mRNA or protein level, which was in line with the network pharmacology analysis results. However, no significant changes in the mRNA and protein expression levels of *ABCG2* by CP treatment were shown in HUA mice. And the expression of *ABCG2* in the small intestine needs further study.

Following the KEGG signal pathway analysis, the mechanisms of CP in the treatment of HUA mainly involved inflammation and apoptosis signaling pathways, including PI3K/Akt, TNF, FoxO, MAPK, HIF-1, TLR, NLRP3, AMPK, and NF- κ B. The PI3K/Akt pathway is a crucial pathway that regulates cell proliferation, cell survival, cell cycle progression, and cancer metabolism (Ocklenburg et al., 2021). Studies have found that in the Uox-knock-out-induced HUA and nephropathy rat line, the PI3K inhibitor 3-MA alleviates kidney injury accompanied by renal fibrosis, macrophage infiltration, and expression of NLRP3 and IL-1 β in injured kidneys (Wu et al., 2021). Furthermore, soluble UA regulates the PI3K/Akt pathway and TLR4-NLRP3 inflammasome and increases the expression of ABCG2 and PDZK1, therefore accelerating the excretion of UA in the intestines and feces (Chen et al., 2018). Emerging evidence has indicated that the NLRP3 inflammasome plays a crucial role in the progression of HUA and kidney inflammation. And our previous study has indicated that dihydroberberine, one of the main metabolites of BBR in the intestinal ecosystem, ameliorates HUA and inflammation by blocking the NLRP3 inflammasome activation in PO/HX-induced hyperuricemic mice (Xu L. Q. et al., 2021). Extracellular UA and MSU have been recognized by TLR2 and TLR4 in gouty arthritis and activate the MAPK, NLRP3 and NF- κ B signaling pathways, thus initiating the inflammatory response (Qing et al., 2014; Xiao et al., 2015). Literature information suggests that Cortex Phellodendron exerts crucial anti-inflammatory effect by inhibiting NF- κ B and MAPK pathways (Choi et al., 2014). In conclusion, CP exerted anti-HUA effect by modulating multiple signaling pathways.

Conclusion

In the present work, a network pharmacology approach combined with *in vitro* experimental validation was integrated to investigate the bioactive ingredients, targets, and pathways of CP against HUA. Our findings indicated that CP exerted potent anti-HUA effect by inhibiting UA production, and possessed nephroprotective effects, at least in part, by inhibition of inflammatory and apoptotic pathways, e.g., PI3K/AKT, TNF, MAPK, TLR, and NLRP3. Although we have used a network pharmacology approach to preliminarily analyze the hub genes involved in the therapeutic effect of CP against HUA, their specific regulation mechanism merits further investigation.

Data availability statement

The original contributions presented in the study are included in the article/Supplementary Material, further inquiries can be directed to the corresponding authors.

Ethics statement

The animal study was reviewed and approved by Animal Ethics Committee of Guangzhou University of Chinese Medicine.

Author contributions

LX, ZS, and QZ participated in the research design; LX, JuC, GL, QY, and JL carried out the experiment; JX, JiC, and YL performed the data analysis; LX wrote the original draft; JuC and JX revised and edited the manuscript; ZS and QZ secured the funding. All authors reviewed and approved the manuscript.

Funding

This work was supported by the National Natural Science Foundation of China (No. 82074082), Natural Science Foundation of Guangdong Province (2022A1515011706), and Guangdong Basic and Applied Basic Research (2021B1515140003).

Conflict of interest

The corresponding author QZ is a joint postdoctoral grant from the Guangzhou University of Chinese Medicine and China Resources Sanjiu Medical and Pharmaceutical Co., Ltd.

The remaining authors declare that the research was conducted in the absence of any commercial or financial relationships that could be construed as a potential conflict of interest.

The reviewer (ZH) declared a shared affiliation with the authors (LX, JuC, JL, GL, QY, YL, JiC, JX, and ZS) at the time of review.

Publisher's note

All claims expressed in this article are solely those of the authors and do not necessarily represent those of their affiliated organizations, or those of the publisher, the editors and the reviewers. Any product that may be evaluated in this article, or claim that may be made by its manufacturer, is not guaranteed or endorsed by the publisher.

Supplementary material

The Supplementary Material for this article can be found online at: <https://www.frontiersin.org/articles/10.3389/fphar.2022.964593/full#supplementary-material>

References

- Akioka, K., Ishikawa, T., Osaka, M., Kadotani, Y., Okugawa, K., Nakano, K., et al. (2017). Hyperuricemia and acute renal failure in renal transplant recipients treated with high-dose mizoribine. *Transpl. Proc.* 49 (1), 73–77. doi:10.1016/j.transproceed.2016.11.015
- Amberger, J. S., Bocchini, C. A., Schiettecatte, F., Scott, A. F., and Hamosh, A. (2015). OMIM.org: Online Mendelian Inheritance in Man (OMIM®), an online catalog of human genes and genetic disorders. *Nucleic Acids Res.* 43, D789–D798. doi:10.1093/nar/gku1205
- Bardin, T., and Richette, P. (2014). Definition of hyperuricemia and gouty conditions. *Curr. Opin. Rheumatol.* 26 (2), 186–191. doi:10.1097/bor.000000000000028
- Becker, M. A., Schumacher, H. R., Jr., Wortmann, R. L., MacDonald, P. A., Eustace, D., Palo, W. A., et al. (2005). Febuxostat compared with allopurinol in patients with hyperuricemia and gout. *N. Engl. J. Med.* 353 (23), 2450–2461. doi:10.1056/NEJMoa050373
- Becker, M. A., Schumacher, H. R., MacDonald, P. A., Lloyd, E., and Lademacher, C. (2009). Clinical efficacy and safety of successful longterm urate lowering with febuxostat or allopurinol in subjects with gout. *J. Rheumatol.* 36 (6), 1273–1282. doi:10.3899/jrheum.080814
- Berger, S. I., and Iyengar, R. (2009). Network analyses in systems pharmacology. *Bioinformatics* 25 (19), 2466–2472. doi:10.1093/bioinformatics/btp465
- Cavalcanti, N. G., Marques, C. D., Lins, E. L. T. U., Pereira, M. C., Régio, M. J., Duarte, A. L., et al. (2016). Cytokine profile in gout: Inflammation driven by IL-6 and IL-18? *Immunol. Invest.* 45 (5), 383–395. doi:10.3109/08820139.2016.1153651
- Chen, C. Y. (2011). TCM Database@Taiwan: The world's largest traditional Chinese medicine database for drug screening *in silico*. *PLoS One* 6 (1), e15939. doi:10.1371/journal.pone.0015939
- Chen, M., Lu, X., Lu, C., Shen, N., Jiang, Y., Chen, M., et al. (2018). Soluble uric acid increases PDZK1 and ABCG2 expression in human intestinal cell lines via the TLR4-NLRP3 inflammasome and PI3K/Akt signaling pathway. *Arthritis Res. Ther.* 20 (1), 20. doi:10.1186/s13075-018-1512-4
- Chen, M. L., Xian, Y. F., Ip, S. P., Tsai, S. H., Yang, J. Y., and Che, C. T. (2010). Chemical and biological differentiation of Cortex Phellodendri chinensis and Cortex Phellodendri amurensis. *Planta Med.* 76 (14), 1530–1535. doi:10.1055/s-0030-1249774
- Choi, Y. Y., Kim, M. H., Han, J. M., Hong, J., Lee, T. H., Kim, S. H., et al. (2014). The anti-inflammatory potential of Cortex phellodendron *in vivo* and *in vitro*: Down-regulation of NO and iNOS through suppression of NF- κ B and MAPK activation. *Int. Immunopharmacol.* 19 (2), 214–220. doi:10.1016/j.intimp.2014.01.020
- Commission, C. P. (2020). *Pharmacopoeia of People's Republic of China*. Beijing: China Medical Science Press, 1.
- Daina, A., Michielin, O., and Zoete, V. (2019). SwissTargetPrediction: Updated data and new features for efficient prediction of protein targets of small molecules. *Nucleic Acids Res.* 47 (W1), W357–W364. doi:10.1093/nar/gkz382
- Dalbeth, N., Merriman, T. R., and Stamp, L. K. (2016). Gout. *Lancet* 388 (10055), 2039–2052. doi:10.1016/s0140-6736(16)00346-9
- Davis, A. P., Grondin, C. J., Johnson, R. J., Sciaky, D., Wiegiers, J., Wiegiers, T. C., et al. (2021). Comparative Toxicogenomics database (CTD): Update 2021. *Nucleic Acids Res.* 49 (D1), D1138–d1143. doi:10.1093/nar/gkaa891
- De Borst, M. H., Prakash, J., Melenhorst, W. B., van den Heuvel, M. C., Kok, R. J., Navis, G., et al. (2007). Glomerular and tubular induction of the transcription factor c-Jun in human renal disease. *J. Pathol.* 213 (2), 219–228. doi:10.1002/path.2228
- de Souza, M. R., de Paula, C. A., Pereira de Resende, M. L., Grabe-Guimarães, A., de Souza Filho, J. D., and Saúde-Guimarães, D. A. (2012). Pharmacological basis for use of *lychnophora trichocarpa* in gouty arthritis: Anti-hyperuricemic and anti-inflammatory effects of its extract, fraction and constituents. *J. Ethnopharmacol.* 142 (3), 845–850. doi:10.1016/j.jep.2012.06.012
- Dong, Y., Hao, L., Fang, K., Han, X. X., Yu, H., Zhang, J. J., et al. (2021). A network pharmacology perspective for deciphering potential mechanisms of action of *Solanum nigrum* L. in bladder cancer. *BMC Complement. Med. Ther.* 21 (1), 45. doi:10.1186/s12906-021-03215-3
- Ferraz-Filha, Z. S., Michel Araújo, M. C., Ferrari, F. C., Dutra, I. P., and Saúde-Guimarães, D. A. (2016). *Tabebuia rosealba*: *In vivo* hypouricemic and anti-inflammatory effects of its ethanolic extract and constituents. *Planta Med.* 82 (16), 1395–1402. doi:10.1055/s-0042-105878
- Hixon, M. L., and Boekelheide, K. (2003). Expression and localization of total Akt1 and phosphorylated Akt1 in the rat seminiferous epithelium. *J. Androl.* 24 (6), 891–898. doi:10.1002/j.1939-4640.2003.tb03141.x
- Hong, Y., Ming-jun, S., Ying, X., Rui-xia, L., Yuan-yuan, W., Hua-zhen, G., et al. (2013). Danqi mixture down-regulates Akt1 expression of kidney tissue in diabetic rats. *Chin. J. Exp. Traditional Med. Formulae* 19 (07), 259–262.
- Hua, J., Huang, P., Zhu, C. M., Yuan, X., and Yu, C. H. (2012). Anti-hyperuricemic and nephroprotective effects of Modified Simiao Decoction in hyperuricemic mice. *J. Ethnopharmacol.* 142 (1), 248–252. doi:10.1016/j.jep.2012.04.052
- Huang, L., Xie, D., Yu, Y., Liu, H., Shi, Y., Shi, T., et al. (2018). TCMID 2.0: A comprehensive resource for TCM. *Nucleic Acids Res.* 46 (D1), D1117–D1120. doi:10.1093/nar/gkx1028
- Ichida, K., Matsuo, H., Takada, T., Nakayama, A., Murakami, K., Shimizu, T., et al. (2012). Decreased extra-renal urate excretion is a common cause of hyperuricemia. *Nat. Commun.* 3, 764. doi:10.1038/ncomms1756
- Jansen, T. L., Perez-Ruiz, F., Tausche, A. K., and Richette, P. (2018). International position paper on the appropriate use of uricosurics with the introduction of lesinurad. *Clin. Rheumatol.* 37 (12), 3159–3165. doi:10.1007/s10067-018-4306-9
- Juan, Y. S., Chuang, S. M., Long, C. Y., Lin, R. J., Liu, K. M., Wu, W. J., et al. (2012). Protein kinase C inhibitor prevents renal apoptotic and fibrotic changes in response to partial ureteric obstruction. *BJU Int.* 110 (2), 283–292. doi:10.1111/j.1464-410X.2011.10805.x
- Kong, L. D., Yang, C., Ge, F., Wang, H. D., and Guo, Y. S. (2004). A Chinese herbal medicine Ermiao wan reduces serum uric acid level and inhibits liver xanthine dehydrogenase and xanthine oxidase in mice. *J. Ethnopharmacol.* 93 (2-3), 325–330. doi:10.1016/j.jep.2004.04.008
- Lee, M. H., Graham, G. G., Williams, K. M., and Day, R. O. (2008). A benefit-risk assessment of benzbromarone in the treatment of gout. Was its withdrawal from the market in the best interest of patients? *Drug Saf.* 31 (8), 643–665. doi:10.2165/0002018-200831080-00002
- Li, W. F., Hao, D. J., Fan, T., Huang, H. M., Yao, H., and Niu, X. F. (2014). Protective effect of chelerythrine against ethanol-induced gastric ulcer in mice. *Chem. Biol. Interact.* 208, 18–27. doi:10.1016/j.cbi.2013.11.011
- Lin, G., Yu, Q., Xu, L., Huang, Z., Mai, L., Jiang, L., et al. (2021). Berberubine attenuates potassium oxonate- and hypoxanthine-induced hyperuricemia by regulating urate transporters and JAK2/STAT3 signaling pathway. *Eur. J. Pharmacol.* 912, 174592. doi:10.1016/j.ejphar.2021.174592
- Luo, J., Wang, X., Jiang, X., Liu, C., Li, Y., Han, X., et al. (2020). Rutaecarpine derivative R3 attenuates atherosclerosis via inhibiting NLRP3 inflammasome-related inflammation and modulating cholesterol transport. *Faseb J.* 34 (1), 1398–1411. doi:10.1096/fj.201900903RRR
- Ma, C. H., Kang, L. L., Ren, H. M., Zhang, D. M., and Kong, L. D. (2015). Simiao pill ameliorates renal glomerular injury via increasing Sirt1 expression and suppressing NF- κ B/NLRP3 inflammasome activation in high fructose-fed rats. *J. Ethnopharmacol.* 172, 108–117. doi:10.1016/j.jep.2015.06.015
- Ma, H., Zhang, Y. F., Wang, J. X., Guo, Y. J., Hu, G. Q., Xie, S. N., et al. (2021). Palmatine attenuates LPS-induced inflammatory response in mouse mammary epithelial cells through inhibiting ERK1/2, P38 and Akt/NF- κ B signalling pathways. *J. Anim. Physiol. Anim. Nutr.* 105 (1), 183–190. doi:10.1111/jpn.13440
- Nakatomi, M., Kanai, M., Nakayama, A., Hishida, A., Kawamura, Y., Ichihara, S., et al. (2019). Genome-wide meta-analysis identifies multiple novel loci associated with serum uric acid levels in Japanese individuals. *Commun. Biol.* 2, 115. doi:10.1038/s42003-019-0339-0
- Niu, X. F., Zhou, P., Li, W. F., and Xu, H. B. (2011). Effects of chelerythrine, a specific inhibitor of cyclooxygenase-2, on acute inflammation in mice. *Fitoterapia* 82 (4), 620–625. doi:10.1016/j.fitote.2011.01.020
- Niu, X., Mu, Q., Li, W., Huang, H., Yao, H., and Li, H. (2014). Protective effects of chelerythrine against lipopolysaccharide-induced endotoxemic shock in mice. *Inflammation* 37 (6), 1968–1975. doi:10.1007/s10753-014-9929-7
- Ocklenburg, T., Neumann, F., Wolf, A., Vogel, J., Göpelt, K., Baumann, M., et al. (2021). In oxygen-deprived tumor cells ERp57 provides radioprotection and ensures proliferation via c-Myc, PLK1 and the AKT pathway. *Sci. Rep.* 11 (1), 7199. doi:10.1038/s41598-021-86658-5
- Pan, Z., Duan, F. J., Wang, Y. H., Zhang, J. B., and Wei, X. H. (2008). Effect of extract of Cortex Phellodendri and atractylodes lancea on hyperuricemia in mice. *Lishizhen Med. Materia Medica Res.* (1), 112–113.
- Perez-Ruiz, F., and Dalbeth, N. (2019). Gout. *Rheum. Dis. Clin. North Am.* 45 (4), 583–591. doi:10.1016/j.rdc.2019.08.001
- Pillinger, M. H., and Mandell, B. F. (2020). Therapeutic approaches in the treatment of gout. *Semin. Arthritis Rheum.* 50, S24–S30. doi:10.1016/j.semarthrit.2020.04.010

- Piñero, J., Ramirez-Anguita, J. M., Saüch-Pitarch, J., Ronzano, F., Centeno, E., Sanz, F., et al. (2020). The DisGeNET knowledge platform for disease genomics: 2019 update. *Nucleic Acids Res.* 48 (D1), D845–D855. doi:10.1093/nar/gkz1021
- Qing, Y. F., Zhang, Q. B., Zhou, J. G., and Jiang, L. (2014). Changes in toll-like receptor (TLR)4-NFκB-IL1β signaling in male gout patients might be involved in the pathogenesis of primary gouty arthritis. *Rheumatol. Int.* 34 (2), 213–220. doi:10.1007/s00296-013-2856-3
- Richette, P., and Bardin, T. (2010). Gout. *Lancet* 375 (9711), 318–328. doi:10.1016/s0140-6736(09)60883-7
- Ru, J., Li, P., Wang, J., Zhou, W., Li, B., Huang, C., et al. (2014). TCMSP: A database of systems pharmacology for drug discovery from herbal medicines. *J. Cheminform.* 6, 13. doi:10.1186/1758-2946-6-13
- Safran, M., Solomon, I., Shmueli, O., Lapidot, M., Shen-Orr, S., Adato, A., et al. (2002). GeneCards 2002: Towards a complete, object-oriented, human gene compendium. *Bioinformatics* 18 (11), 1542–1543. doi:10.1093/bioinformatics/18.11.1542
- Shi, B., Li, S., Ju, H., Liu, X., Li, D., and Li, Y. (2019). Protein kinase C inhibitor chelerythrine attenuates partial unilateral ureteral obstruction induced kidney injury in neonatal rats. *Life Sci.* 216, 85–91. doi:10.1016/j.lfs.2018.11.025
- Shi, H., Liu, J., and Gao, H. (2021). Benzo(a)pyrene induces oxidative stress and inflammation in human vascular endothelial cells through AhR and NF-κB pathways. *Microvasc. Res.* 137 (1), 104179. doi:10.1016/j.mvr.2021.104179
- Trautwein, E. A., and Demonty, I. (2007). Phytosterols: Natural compounds with established and emerging health benefits. *OCL - Oilseeds Fats, Crops Lipids* 14 (5), 259–266. doi:10.1051/ocl.2007.0145
- UniProt Consortium (2019). UniProt: A worldwide hub of protein knowledge. *Nucleic Acids Res.* 47 (D1), D506–D515. doi:10.1093/nar/gky1049
- Wang, K. X., Gao, Y., Lu, C., Li, Y., Zhou, B. Y., Qin, X. M., et al. (2020). Uncovering the complexity mechanism of different formulas treatment for rheumatoid arthritis based on a novel network pharmacology model. *Front. Pharmacol.* 11, 1035. doi:10.3389/fphar.2020.01035
- Wang, X., Wang, C. P., Hu, Q. H., Lv, Y. Z., Zhang, X., Ouyang, Z., et al. (2010). The dual actions of Sanmiao wan as a hypouricemic agent: Down-regulation of hepatic XOD and renal mURAT1 in hyperuricemic mice. *J. Ethnopharmacol.* 128 (1), 107–115. doi:10.1016/j.jep.2009.12.035
- Wei, Z., Xu, C., Liu, S., Song, F., Liu, Z., and Qu, X. (2018). Metabonomics study of the effects of traditional Chinese medicine formula Erniaowan on hyperuricemic rats. *J. Sep. Sci.* 41 (2), 560–570. doi:10.1002/jssc.201700985
- Woodward, O. M., Köttgen, A., Coresh, J., Boerwinkle, E., Guggino, W. B., and Köttgen, M. (2009). Identification of a urate transporter, ABCG2, with a common functional polymorphism causing gout. *Proc. Natl. Acad. Sci. U. S. A.* 106 (25), 10338–10342. doi:10.1073/pnas.0901249106
- Wu, H. H., Lv, X., Guo, L. Z., and Ji, B. (2019). Treatment of acute gout attack with integrated traditional Chinese and western medicine. *J. Changchun Univ. Chin. Med.* 035 (001), 73–75.
- Wu, M., Ma, Y., Chen, X., Liang, N., Qu, S., and Chen, H. (2021). Hyperuricemia causes kidney damage by promoting autophagy and NLRP3-mediated inflammation in rats with urate oxidase deficiency. *Dis. Model. Mech.* 14 (3), dmm048041. doi:10.1242/dmm.048041
- Wu, S., Yang, Y., Li, F., Huang, L., Han, Z., Wang, G., et al. (2018). Chelerythrine induced cell death through ROS-dependent ER stress in human prostate cancer cells. *Oncotargets Ther.* 11, 2593–2601. doi:10.2147/ott.s157707
- Xian, Y. F., Lin, Z. X., Ip, S. P., Su, Z. R., Chen, J. N., and Lai, X. P. (2013). Comparison the neuroprotective effect of Cortex Phellodendri chinensis and Cortex Phellodendri amurensis against beta-amyloid-induced neurotoxicity in PC12 cells. *Phytomedicine* 20 (2), 187–193. doi:10.1016/j.phymed.2012.09.028
- Xiao, J., Zhang, X. L., Fu, C., Han, R., Chen, W., Lu, Y., et al. (2015). Soluble uric acid increases NALP3 inflammasome and interleukin-1β expression in human primary renal proximal tubule epithelial cells through the Toll-like receptor 4-mediated pathway. *Int. J. Mol. Med.* 35 (5), 1347–1354. doi:10.3892/ijmm.2015.2148
- Xu, L. Q., Lin, G. S., Yu, Q. X., Li, Q. P., Mai, L. T., Cheng, J. J., et al. (2021). Anti-hyperuricemic and nephroprotective effects of dihydroberberine in potassium oxonate- and hypoxanthine-induced hyperuricemic mice. *Front. Pharmacol.* 12, 645879. doi:10.3389/fphar.2021.645879
- Xu, Y., Cao, X., Zhao, H., Yang, E., Wang, Y., Cheng, N., et al. (2021). Impact of camellia japonica bee pollen polyphenols on hyperuricemia and gut microbiota in potassium oxonate-induced mice. *Nutrients* 13 (8), 2665. doi:10.3390/nu13082665
- Yang, C., Zhu, J. X., Wang, Y., Weng, Y. L., and Kong, L. D. (2005). Effects of processing phellodendron amurense with salt on anti-gout. *China J. Chin. Materia Medica* 30 (2), 145–148.
- Zhang, R., Zhan, S., Li, S., Zhu, Z., He, J., Lorenzo, J. M., et al. (2018). Anti-hyperuricemic and nephroprotective effects of extracts from *Chaenomeles sinensis* (Thouin) Koehne in hyperuricemic mice. *Food Funct.* 9 (11), 5778–5790. doi:10.1039/c8fo01480a
- Zhang, T., Li, H., Shi, J., Li, S., Li, M., Zhang, L., et al. (2016). p53 predominantly regulates IL-6 production and suppresses synovial inflammation in fibroblast-like synoviocytes and adjuvant-induced arthritis. *Arthritis Res. Ther.* 18 (1), 271. doi:10.1186/s13075-016-1161-4
- Zhang, Z. F., Guo, Y., Zhang, J. B., and Wei, X. H. (2011). Induction of apoptosis by chelerythrine chloride through mitochondrial pathway and Bcl-2 family proteins in human hepatoma SMMC-7721 cell. *Arch. Pharm. Res.* 34 (5), 791–800. doi:10.1007/s12272-011-0513-5
- Zheng, W., Qiu, L., Wang, R., Feng, X., Han, Y., Zhu, Y., et al. (2015). Selective targeting of PPARγ by the natural product chelerythrine with a unique binding mode and improved antidiabetic potency. *Sci. Rep.* 5, 12222. doi:10.1038/srep12222